MNRAS **000**, 1–13 (2018) Preprint 24 October 2018 Compiled using MNRAS LATEX style file v3.0

A Simple Non-equilibrium Feedback Model for Galaxy-Scale Star Formation: Delayed Feedback and SFR Scatter

Matthew E. Orr[1]⋆, Christopher C. Hayward[2], Philip F. Hopkins[1]
[1] *TAPIR, Mailcode 350-17, California Institute of Technology, Pasadena, CA 91125, USA*
[2] *Center for Computational Astrophysics, Flatiron Institute, 162 Fifth Avenue, New York, NY 10010, USA*

Draft date: 24 October 2018

ABSTRACT

We explore a class of simple non-equilibrium star formation models within the framework of a feedback-regulated model of the ISM, applicable to kiloparsec-scale resolved star formation relations (e.g. Kennicutt-Schmidt). Combining a Toomre-Q-dependent local star formation efficiency per free-fall time with a model for delayed feedback, we are able to match the normalization and scatter of resolved star formation scaling relations. In particular, this simple model suggests that large (∼dex) variations in star formation rates (SFRs) on kiloparsec scales may be due to the fact that supernova feedback is not instantaneous following star formation. The scatter in SFRs at constant gas surface density in a galaxy then depends on when we observe its star-forming regions at various points throughout their collapse/star formation "cycles". This has the following important observational consequences: (1) the scatter and normalization of the Kennicutt-Schmidt relation are insensitive to the local (small-scale) star formation efficiency, (2) but depletion times and velocity dispersions in the gas are; (3) the scatter in the Kennicutt-Schmidt relation is a sensitive probe of the feedback timescale; (4) even in a model where $\tilde{Q}_{\rm gas}$ deterministically dictates star formation, time lags destroy much of the observable correlation between SFR and $\tilde{Q}_{\rm gas}$.

Key words: galaxies: star formation – galaxies: evolution.

1 INTRODUCTION

One of the fundamental characteristics of star formation is that it is globally inefficient: galaxies convert only a few per cent of their cold gas reservoirs into stars per dynamical time (Kennicutt, Jr. et al. 2007). As to why this is the case, there are two broad frameworks for regulating star formation in galaxies: dynamics and feedback. Dynamical regulation argues that stars form as rapidly as they are able, but that dynamical processes such as turbulent shear, differential rotation, or gas expansion behind spiral arms govern the fraction of gas with conditions favorable to star formation (Saitoh et al. 2008; Robertson & Goldreich 2012; Elmegreen & Hunter 2015; Semenov et al. 2017). In this regime, star formation efficiency is low locally, in complement with its global value. Feedback regulation argues instead that star formation could be locally highly efficient in regions which are actually collapsing without local feedback present, but that stellar feedback (usually in addition to dynamical processes), in the form of ionizing radiation or supernova explosions, heat and stir the ISM, preventing further star formation in most regions and times (Thompson et al. 2005; Murray et al. 2010; Ostriker et al. 2010; Shetty & Ostriker 2012a; Hopkins et al. 2014; Kim & Ostriker 2015b; Hopkins et al. 2018, among others).

Within the framework of feedback-regulation there have been several related models describing various star formation 'laws', including the "outer disk" model of Ostriker & Shetty (2011), the "two-zone" theory of Faucher-Giguere et al. (2013), and radiation pressure supported models like Thompson et al. (2005), to name a few. Particular focus has been laid on models involving turbulent support of the ISM, as thermal heating processes become relatively ineffective at regulating star formation for gas surface densities above $\sim$10 $M_\odot$ pc^{-2}, where a self-shielded component of the ISM necessarily develops (Krumholz et al. 2009a,b; Hayward & Hopkins 2017). Broadly, turbulently-regulated models incorporate some metallicity dependence (often having to do with the metallicity dependence of the efficiency of SNe momentum coupling, Martizzi et al. 2015), local gas fraction (or

⋆ E-mail: meorr@caltech.edu

stellar surface density, Ostriker & Shetty 2011), or local gas scale height dependence (Faucher-Giguere et al. 2013), in setting the equilibrium star formation rate.

These models have found general agreement with the *mean* observed star formation rates (either galaxy-integrated or as a function of radius) in nearby galaxies. However, observational studies of the spatially-resolved (at ∼kpc scales) Kennicutt-Schmidt relation have apparently-characteristic $\pm 2\sigma$ scatters of $\sim 1-2$ dex in star formation rates at constant gas surface densities (Bigiel et al. 2008; Leroy et al. 2008; Bigiel et al. 2010; Leroy et al. 2013, 2017), with a similar scatter having been seen in cosmological simulations (Orr et al. 2018). Generally, these variations in star formation rates within individual galaxies at constant gas surface density are not readily explained by local variations in metallicity. For instance, at fixed galactocentric radii in discs, gas metallicity is seen to vary at $\lesssim 0.1$ dex levels (Ho et al. 2017), whereas gas surface densities can vary by more than 2 dex, requiring SFE $\propto Z^{20}$ (not seen observationally, or having a theoretical basis for being the case) to explain SFR variations independent of gas surface densities. Nor are metallicity gradients large enough to explain the scatter, as generally gas surface densities fall far more quickly than metallicities (Ma et al. 2017). Gas fractions, too, appear lacking in their ability to drive large scatter in SFRs at constant gas surface density *within* galaxies (Leroy et al. 2013).

This large scatter could suggest that we are still missing some critical physics in our models, or observationally our inferred star formation rates and gas surface densities are introducing much larger errors than usually appreciated. From the side of theory, that we are roughly matching star formation rate distributions, and their scatter in particular, in cosmological simulations is heartening (Orr et al. 2018) and suggests the feedback physics included in simulations like those of Hopkins et al. (2014, 2018) or Agertz & Kravtsov (2015) are close to sufficient. On the side of observations, there remains work to be done in converging on conversion factors between luminosities or line widths, and star formation rates and gas masses but it is unlikely that these factors randomly vary by ~ 2 dex in neighboring kpc-patches of ISM (Kennicutt & Evans 2012; Narayanan et al. 2012; Bolatto et al. 2013).

Another possible resolution is that rather than star formation being locked to a 'law' dependent on gas surface density, there is some "intrinsic" uncertainty to it (Calzetti et al. 2012; Kruijssen & Longmore 2014; Kruijssen et al. 2018). Kruijssen & Longmore (2014) argue that star formation relations like that of the Kennicutt-Schmidt relation must necessarily break down on some scale due to the overlap (or lack thereof) both temporally and spatially between tracers of dense gas and star formation, and that scatter in these relations is a necessary consequence. But to what extent does the framework of feedback-regulation itself provide an intrinsic scatter to the predicted equilibrium star formation rates? After all, feedback is not instantaneous with star formation, as ionizing radiation is injected for upwards of 10 Myr (Leitherer et al. 1999), supernova feedback is not felt for the first ~ 5 Myr, and then continues stochastically for ~ 30 Myr (Agertz et al. 2013). The timescales for feedback injection are not coincidentally on the order of the lifetimes of star forming regions themselves in the feedback regulated model (Oklopčić et al. 2017; Semenov et al. 2018; Grudić et al. 2018). Star formation *equilibrium* need not be expected, even at the 10^6 $M_\odot$ GMC scale.

Table 1. Summary of variables used in this paper

Symbol	Definition
$\dot{\Sigma}_\star$	Star formation rate surface density
Σ_g	Total gas surface density
$f_{\rm sf}$	Gas mass fraction in star-forming phase
f_g	Fraction of disk mass in gas
ρ_0	Disk mid-plane volume mass density
t_d	Delay timescale for the injection of feedback
δt_d	Period of feedback injection
α	Slope of power law for delay-time distribution of Type-II SNe
H	Gas scale height
G	Newtonian gravitational constant
$P/m_\star$	Characteristic feedback momentum per mass of stars formed
$t_{\rm eddy}$	Eddy (disk scale height) crossing time
$\langle\epsilon_{\rm sf}\rangle$	Average star formation efficiency per eddy time (here, GMC-scale average value)
$\bar{\epsilon}_{\rm sf}$	Star formation efficiency per orbital dynamical time
$\tilde{Q}_{\rm gas}$	Modified Toomre-Q gas stability parameter
Ω	Local orbital dynamical time
σ	Turbulent gas velocity dispersion (3-D)

Indeed others (Benincasa et al. 2016; Torrey et al. 2017; Semenov et al. 2018) have argued that while star formation might be in "static equilibrium" (i.e. steady state) in some averaged sense, that it is locally in some *dynamical* equilibrium where the ISM is in a constant cycle of collapse, star formation, and cloud destruction/feedback. It is thus never instantaneously in local equilibrium, and is constantly oscillating between those phases (Benincasa et al. 2016; Semenov et al. 2017, 2018).

In this paper, within the framework of feedback-regulation, we explore a simple non-equilibrium star-formation model, which expands upon these previous works. Critically, we explore models wherein there is a non-trivial delay time, with respect to the local dynamical time, between the formation of young stars and the injection of the bulk of their feedback into the ISM. We investigate the results of including a time dependence between the criteria for star formation being met, and its effects being felt- in particular, the ability to explain significant (∼dex) scatter in star formation rates in resolved galaxy scaling relations. We explore how this ultimately leads to scatter in the Kennicutt-Schmidt relation, but also a number of non-intuitive effects for observed galaxy scalings of quantities that enter the model.

2 MODEL

In a previous work (Orr et al. 2018), we explored the ability of turbulent energy injection, in the form of the effects of Type II SNe, to explain the equilibrium value of the Kennicutt-Schmidt relation in the FIRE simulations at gas surface densities $\gtrsim 10$ $M_\odot$ pc^{-2} (similar in derivation to Ostriker & Shetty 2011; Faucher-Giguere et al. 2013; Hay-

ward & Hopkins 2017). The predicted equilibrium was in good agreement with the median values seen in the simulations, which were themselves in good agreement with the observed atomic+molecular formulation of the Kennicutt-Schmidt relation. However, the $\pm 2\sigma$ scatter seen, on the order of $\sim 1.5-2$ dex, was not explained fully by local environmental variations, e.g. metallicity, dynamical time, or stellar surface density. There appeared to be an intrinsic scatter of $\gtrsim$dex to the star formation rate distribution seen at any given gas surface density.

To explore the physical processes that cause scatter in resolved star formation scaling relations in disk environments within individual galaxies, let us consider a patch of the ISM where the turbulent velocity dispersion is taken to be roughly isotropic, where we assume

$$\sigma^2 = \sigma_R^2 + \sigma_z^2 + \sigma_\phi^2 \approx 3\sigma_R^2 \, , \tag{1}$$

or $\sigma \approx \sqrt{3}\sigma_R$ where σ is the overall gas velocity dispersion, and the subscripted σ's denote the velocity dispersions in the radial, vertical (i.e. line of sight in face-on galaxies), and tangential directions, respectively.

In the framework of a supersonic turbulent cascade, the largest eddies carry the bulk of the energy and momentum to first order, and we can take the momentum per area in the turbulent/random motion of the gas to be the velocity dispersion at the largest scale (here, the gas disk scale height H) times the gas mass surface density Σ_g, that is $P_{turb} = \Sigma_g \sigma$. The timescale for the dissipation t_{diss} of this turbulent momentum is roughly the eddy turnover time $t_{\rm eddy}$, which is $t_{\rm eddy} \approx H/\sigma_z$. If we assume that the gas disk is embedded in the potential of stellar disk with a larger scale height, as is seen in the Milky-Way with the thin gas disk having a characteristic height of $\sim$ 100 pc embedded within the larger $\sim$ 300 pc stellar scale height (Gilmore & Reid 1983; Scoville & Sanders 1987), and that the gravitational acceleration near the mid-plane due to the local disk mass itself is of the form $4\pi G\rho_0 z$, where ρ_0 is the mid-plane density (gas + stars), and the external potential[1] introduces a vertical acceleration component of $v_c^2 z/R^2 = \Omega^2 z$ (where $\Omega \equiv v_c/R$), then the vertical (z) density profile is a Gaussian with a characteristic scale height of

$$H = \frac{\sigma_z}{\Omega + \sqrt{4\pi G\rho_0}} \, . \tag{2}$$

So, $t_{diss} \approx t_{\rm eddy} \approx H/\sigma_z \approx 1/(\Omega + \sqrt{4\pi G\rho_0})$. In the absence of stellar feedback, the turbulent momentum of this patch of the ISM would be expected to exponentially decay as

$$\dot{P}_{turb} = -\Sigma_g \sigma / t_{diss} = -P_{turb}(\Omega + \sqrt{4\pi G\rho_0}) \, , \tag{3}$$

which admits a solution for gas velocity dispersions of $\sigma(t) = \sigma_0 \exp\left(-t(\Omega + \sqrt{4\pi G\rho_0})\right)$.

[1] Here, the local dark matter contribution is implicitly included, whereas it is ignored for simplicity in the disk self-gravity acceleration term as the baryonic component dominates the thin disk mass in galaxies. Our model could be extended to gas-rich dwarfs or high-redshift galaxies with poorly defined disks, but would require a different formulation of gas scale-lengths/heights.

2.1 Equilibrium Model of Instantaneous Feedback Injection in Disk Environments

However, feedback from massive stars acts to inject momentum back into the ISM at the largest scales (i.e. disk scale heights, Padoan et al. 2016). Taking the characteristic momentum injected per mass of young stars formed to be $P/m_\star$, we can establish an equilibrium for σ if we balance the rate of momentum injection from feedback, $\dot{\Sigma}_\star P/m_\star$, with the turbulence dissipation rate in Eq. 3, that is,

$$\left(\frac{P}{m_\star}\right)\dot{\Sigma}_\star = \Sigma_g \sigma(\Omega + \sqrt{4\pi G\rho_0}) \, . \tag{4}$$

Arguing that star-forming disks are marginally stable against gravitational instabilities, we invoke a modified[2] Toomre-Q criterion dictating instantaneous gas stability (Toomre 1964),

$$\tilde{Q}_{\rm gas} = \frac{\sqrt{2}\sigma_R \Omega}{\pi G \Sigma_{disk}} \, , \tag{5}$$

where $\Sigma_{\rm disk} = \Sigma_g + \gamma\Sigma_\star$ is the mid-plane surface density, including the stellar component (with the factor γ accounting for the effective fraction of stellar mass within a gas scale height, $\gamma = 1 - \exp(-H/H_\star)$). We substitute this Toomre-Q into Eq. 4 for σ, recovering the Kennicutt-Schmidt relation for a turbulently supported ISM,

$$\dot{\Sigma}_\star = \pi G \tilde{Q}_{\rm gas} \sqrt{\frac{3}{2}} \frac{\Sigma_g \Sigma_{disk}}{P/m_\star} \left(1 + \frac{\sqrt{4\pi G\rho_0}}{\Omega}\right) \, . \tag{6}$$

Further, we can calculate the "global star formation efficiency", i.e. the fraction of the gas mass converted to stars per orbital dynamical time, $\bar{\epsilon}_{\rm sf} \equiv \dot{\Sigma}_\star / \Sigma_g \Omega$, to be

$$\bar{\epsilon}_{\rm sf} = \pi G \tilde{Q}_{\rm gas} \sqrt{\frac{3}{2}} \frac{\Sigma_{disk}(\Omega + \sqrt{4\pi G\rho_0})}{(P/m_\star)\Omega^2} \, . \tag{7}$$

We take $\tilde{Q}_{\rm gas}$ to be a constant, assuming a value near or slightly below one, and consider the case in which the disk is not strongly self-gravitating (likely, with the marginal stability of $\tilde{Q}_{\rm gas} \approx 1$), such that $\Omega >> \sqrt{4\pi G\rho_0}$; these two relations boil down to a description of gas surface density and mass fraction and a representation of the ratio of disk surface density to inverse dynamical time, respectively:

$$\dot{\Sigma}_\star = \pi G \sqrt{\frac{3}{2}} \frac{\Sigma_g \Sigma_{disk}}{P/m_\star} \quad \& \quad \bar{\epsilon}_{\rm sf} = \pi G \sqrt{\frac{3}{2}} \frac{\Sigma_{disk}}{\Omega P/m_\star} . \tag{8}$$

One deficiency of this model of feedback regulation lies in the calibration of the strength of feedback to isolated Type-II SNe simulations (e.g., Kim & Ostriker 2015a; Martizzi et al. 2015). Generally, this overlooks the variation in effective feedback coupling due to the local environment. Especially for predictions regarding the line of sight velocity dispersions, the potential saturation or "venting" of feedback after SNe remnants (super-bubbles or otherwise) break out of the disk plane is a possible concern (Fielding et al. 2017). We do not explore the effects of feedback saturation here, but they warrant further exploration within the

[2] This is not the 'real' two component Toomre-Q (Rafikov 2001), but is a much simplified version that is sufficiently accurate for our purposes (using the full two-component Q makes little difference to our numerical calculations but prevents us from writing simple analytic expressions).

framework of simple analytic models (these effects are self-consistently handled in galaxy simulations that resolve disk and supernova remnants in the snowplow phase).

2.2 Non-equilibrium Model of Feedback Injection in Disk Environments

The model derived in §2.1 is an equilibrium model, which assumes that feedback injection is statically balanced with the dynamical/dissipation rate. However, we might consider here that the departures from equilibrium occurring on the feedback delay timescale are important for setting the scatter seen in $\dot{\Sigma}_\star$ at constant Σ_g in the Kennicutt-Schmidt relation, and at constant $\Sigma_g\Omega$ for the Elmegreen-Silk relation, as well as in σ_z—$\dot{\Sigma}_\star$ space. We will explicitly consider only delayed feedback (i.e. Type-II SNe) in this model.[3]

Rather than holding the turbulent velocity dispersion σ constant in time, we allow it to vary, defining the behavior of its derivative $\dot{\sigma}$ as,

$$\dot{\sigma} = \dot{\sigma}_{\rm SNe} - \sigma/t_{\rm eddy} \ , \tag{9}$$

where $\dot{\sigma}_{\rm SNe}$ is the term explicitly following the current injection of SNe feedback momentum due to past star formation (see Eq. 10, below), and the $\sigma/t_{\rm eddy}$ term accounts for the exponential decay of supersonic turbulence on roughly an eddy crossing time (Eq. 3). We ignore the fraction of turbulent momentum "locked away" into stars (equivalent to a $\sigma\dot{\Sigma}_g$ term) as the term is negligible with the depletion time of gas typically on the order of ∼Gyr in galaxies (Leroy et al. 2008).

Developing a form for $\dot{\sigma}_{\rm SNe}$, we consider that Type-II SNe feedback from a given star formation event is injected after a delay time t_d, and over a period δt_d, corresponding to the lifetime of the most massive star formed, and the time until the least massive star to undergo core-collapse does so thereafter. Furthermore, convolving the number of stars of a given mass with their lifetimes produces a shallow power-law distribution in time over which SNe occur after a star formation event, such that $dN_{SNII}/dt \propto t^{-\alpha}$ (see Appendix A for a more detailed derivation). These quantities, t_d, δt_d, and α, are reasonably known (see Appendix A), and we adopt fiducial values in this paper of 4 Myr, 36 Myr, and 0.46, respectively. As such, the governing equation for $\dot{\sigma}_{\rm SNe}$ takes the form

$$\Sigma_{\rm g}\dot{\sigma}_{\rm SNe} = (P/m_\star)\chi \int_{t_d}^{t_d+\delta t_d} \frac{\dot{\Sigma}_\star(t-t')}{t'^\alpha} dt' \ , \tag{10}$$

where $P/m_\star$ here is the momentum injected by Type-II SNe event per mass of young stars (as opposed to from all sources of feedback as in § 2.1), and χ is a normalization factor such that for a constant star formation rate the integral leaves $\dot{\Sigma}_\star$ unchanged. We adopt a fiducial value of $P/m_\star = 1250$ km/s (roughly the average between the homogenous and inhomogenous ISM results of Martizzi et al. 2015), and explore the effects of varying the strength of SNe feedback in § 3.1.

It is then necessary to formulate a model for the rate at which star formation proceeds, as a function of the current state of the ISM, as we now consider $\dot{\Sigma}_\star$ to drive $\dot{\sigma}$, rather than being purely in a static equilibrium with the turbulent dissipation.

Taking the large-scale marginal gas stability as a key parameter in setting the current rate of star formation, we invoke a simple "two-phase" model of the ISM, which is instantaneously dependent on the Toomre-Q parameter of the gas disk. Let us assume that some fraction of the gas is in a star-forming phase $f_{\rm sf}$ (i.e. marginally gravitationally-bound gas), with the remaining mass in a non-star-forming phase. As explored analytically by Hopkins (2013), supersonic turbulence drives parcels of gas to randomly walk in log-density space such that a fraction (here, $f_{\rm sf}$) are driven to sufficient densities such that local collapse (i.e. leakage) occurs even if the global value of $\tilde{Q}_{\rm gas}$ exceeds the critical threshold for gravitational instabilities Q_0[4]. Following the rationale of Faucher-Giguere et al. (2013, see their Appendix C), adapting the calculations of Hopkins (2013), we argue that the mass fraction of gas susceptible to gravitational collapse ($f_{\rm sf}$), which subsequently would be considered in some stage of "star-forming", is functionally dependent on Toomre-Q, with an adopted power-law form of,

$$f_{\rm sf}(\tilde{Q}_{\rm gas}) = f_{\rm sf}^0 \left(\frac{Q_0}{\tilde{Q}_{\rm gas}}\right)^\beta \ , \tag{11}$$

for values $\tilde{Q}_{\rm gas} > Q_0$, and is a constant $f_{\rm sf}^0$ for $\tilde{Q}_{\rm gas} < Q_0$, where $f_{\rm sf}^0$ is the maximal fraction of gas in the star-forming phase, Q_0 represents the Toomre-Q stability threshold, and β accounts for the "stiffness" of that threshold. Further, as $\tilde{Q}_{\rm gas}$ evolves (in this model, through evolution purely in σ) smoothly in time, the roll-on (or off, if $\dot{\sigma} > 0$) can also be thought to implicitly parameterize our ignorance in how and at what rate GMCs assemble (for $\dot{\sigma} > 0$, this can approximate ionizing radiation and winds dispersing dense material). In Hopkins (2013), the stiffness of the instability threshold ($\sim \beta$, here) was inversely dependent on the Mach number $\mathcal{M}$ of the turbulence– intuitive, as larger Mach numbers yield a broader log-normal density distribution, increasing the amount of gas above a given density relative to the mean gas density, hence softening the effective gravitational instability threshold. Here, taking $\mathcal{M} \sim \sigma/c_s$, where c_s is the speed of sound for $\sim$ 300 K molecular gas, and $\tilde{Q}_{\rm gas} \sim$ constant, we thus have $\mathcal{M} \propto \sigma \propto \Sigma_g$. And so, in our model at a given gas surface density we adopt a stiffness $\beta = -2\log(\Sigma_g/{\rm M}_\odot{\rm pc}^{-2}) + 6$, proportional to the Mach number-dependent stiffness fit by (Faucher-Giguere et al.

[3] Although prompt feedback (e.g. radiation pressure and stellar winds) injects a similar amount of momentum per mass of young stars over their lifetimes (Agertz et al. 2013), the 'characteristic' velocity at which this momentum couples to the ISM on large scales is lower by a factor of 20 or so, compared to SNe feedback (Murray et al. 2010; Faucher-Giguere et al. 2013). As we consider here the ability of feedback to regulate the disk scale properties that regulate star formation 'from the top down', we neglect explicitly treating the prompt feedback effects in our model. Instead, we implicitly incorporate its effects regulating the efficiencies of cloud-scale, < 100 pc, star formation in our "GMC-scale" SF efficiency model (Grudić et al. 2018).

[4] This is just a formal calculation of the log-normal density distribution of gas in supersonic turbulence. It is to say: turbulence is able to dynamically replenish the fraction of gas in a log-normal density distribution that is above some critical threshold for self-gravity and collapse.

Table 2. Fiducial Model Parameters and Disk Conditions

Parameter	Quantity	Fiducial Value
Toomre-Q Threshold	Q_0	1.0
Max. star-forming fraction	$f_{\rm sf}^0$	0.3
Average SF efficiency	$\langle\epsilon_{\rm sf}\rangle$	0.025
Feedback Strength	$P/m_\star$	1250 km/s
Feedback Delay Time	t_d	5 Myr
Feedback Duration	δt_d	30 Myr
Power law slope of Type-II SNe delay time distribution	α	0.46
Orbital Dynamical Time	Ω	35 Gyr^{-1}
Disk Gas Fraction	f_g	0.33
Stellar Thick Disk Fraction	$f_{\rm thick}$	0.33
Stellar Disk height (thin)	$H_{\rm thin,\star}$	350 pc
Stellar Disk height (thick)	$H_{\rm thick,\star}$	1000 pc

2013), and substantiated by the observational findings relating Σ_g and $\mathcal{M}$ of Federrath et al. (2017).

Arguing that a ∼kpc-sized patch of the ISM likely incorporates a large enough number of $\lesssim$100 pc clouds so as to approach an average behavior in terms of their individual evolutionary states (Schruba et al. 2010; Calzetti et al. 2012; Kruijssen & Longmore 2014), we then adopt a ∼kpc-scale star formation rate of

$$\dot{\Sigma}_\star(t) = \langle\epsilon_{\rm sf}\rangle\, f_{\rm sf}(\tilde{Q}_{\rm gas}(t))\Sigma_g/t_{\rm eddy} \tag{12}$$

where $f_{\rm sf}(\tilde{Q}_{\rm gas}(t))\Sigma_g$ is the mass of gas in the star-forming state (per area), $\langle\epsilon_{\rm sf}\rangle$ is the average star formation efficiency per eddy-crossing time (fiducially, 0.025, in line with cloud-scale efficiencies discussed in Elmegreen 2018), and $t_{\rm eddy}$ is the eddy-crossing time. As the quickest instabilities to grow are at the largest scales, the largest being that of the disk scale height itself, the effective free-fall time of gas at the mid-plane density is equivalent to the eddy crossing time $t_{\rm eddy}$ up to an order unity factor (since $t_{ff} \sim 1/\sqrt{G\rho_0} \sim t_{\rm eddy}$). Again, emphasizing that we defined our efficiency $\langle\epsilon_{\rm sf}\rangle$ (taken to be a constant) as a kpc-scale average quantity, $\langle\epsilon_{\rm sf}\rangle \equiv \left\langle \dot{M}_\odot t_{\rm eddy}/M_{\rm GMC} \right\rangle$. It is analogous to a GMC-scale average star formation efficiency, and as such is unable to distinguish between high or low efficiency star formation modes on smaller scales (e.g. efficiencies calculated on the basis of higher density gas tracers like HCN).

The fiducial values of the physical quantities and common initial conditions included in the evolution of our model– essentially the behavior of the PDE for σ, Eq. 9, are enumerated in Table 2. The initial condition of the gas in the model, in all cases presented here, is taken to be $\tilde{Q}_{\rm gas}(t=0) = Q_0 + 1$ (and its corresponding velocity dispersion σ) for the given Σ_g, embedded within static stellar disk with thin and thick components having scale heights of 350 and 1000 pc, respectively, and a relative mass fraction $f_{\rm thick} \equiv \Sigma_{\rm thick,\star}/(\Sigma_{\rm thick,\star} + \Sigma_{\rm thin,\star}) = 0.33$.

2.2.1 *Connecting $\dot{\Sigma}_\star$, Σ_g with Observables*

Except for the nearest star forming regions, (where young star counts or protostellar cores can be used as proxies), observers rarely have true estimates for the 'instantaneous' star formation rate of a star forming region. As such, we must connect our 'instantaneous' star formation rate with observables like Hα, which are used as average measures of star formation over a recent period of time ∼ 10 Myr. For this reason, when we make attempts to compare with observational star formation relations, we average the instantaneous star formation rate $\dot{\Sigma}_\star$ over the last 10 Myr (see Appendix B for how our results vary with the averaging window). To compare our gas surface densities with observations, we take our gas mass surface density Σ_g to be the atomic+molecular hydrogen gas, correcting them for Helium mass with a factor of 0.75.

In panels where we plot the Kennicutt-Schmidt relation, we compare results of our simple model with resolved Kennicutt-Schmidt observations from Bigiel et al. (2008) (light and dark grey shaded regions in background). We correct the gas surface densities in their data with a variable $X_{\rm CO}$ fit from Narayanan et al. (2012). Where we plot depletion time against gas stability (Toomre-Q), we compare with the results of Leroy et al. (2008) (light and dark grey shaded regions in background).

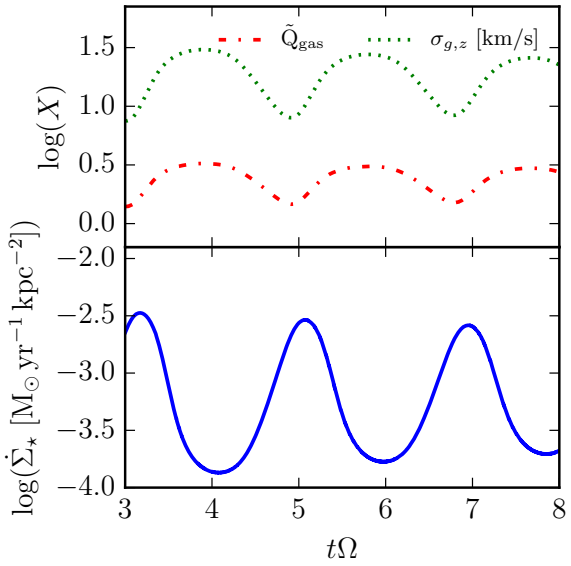

Figure 1. Logarithmic values of star formation rate surface density (solid blue line; 10-Myr-averaged rate), local $\tilde{Q}_{\rm gas}$ (dash-dotted red line), and gas velocity dispersion (dotted green line, units: km/s) for a period of five dynamical times in our fiducial model gas patch (for fiducial model parameters, see Table 2) with $\Sigma_g = 15$ M$_\odot$ pc^{-2} and $\Sigma_\star = 35$ M$_\odot$. The SFR and velocity dispersion maintain stable, albeit slowly decaying, cycles after approximately one dynamical time $\tau_{\rm dyn} \sim \Omega^{-1} \sim 30$ Myr.

3 RESULTS

The simple model produces relatively stable cycles of star formation, inflation and decay of gas velocity dispersions, and variation in the values of the Toomre-Q parameter, as seen in Figure 1 for our set of fiducial values of physical parameters, with disk surface densities and conditions chosen to match the solar circle ($\Sigma_g = 15$ M$_\odot$ pc^{-2}, $\Sigma_\star = 35$ M$_\odot$ pc^{-2}, and $\Omega = 35$ Gyr^{-1} McKee et al. 2015). As star formation is slow and inefficient (gas depletion times are $\gtrsim$ Gyr here), and given the fact that we do not include some gas outflow term, we do not allow Σ_g or $\Sigma_\star$ to vary in the

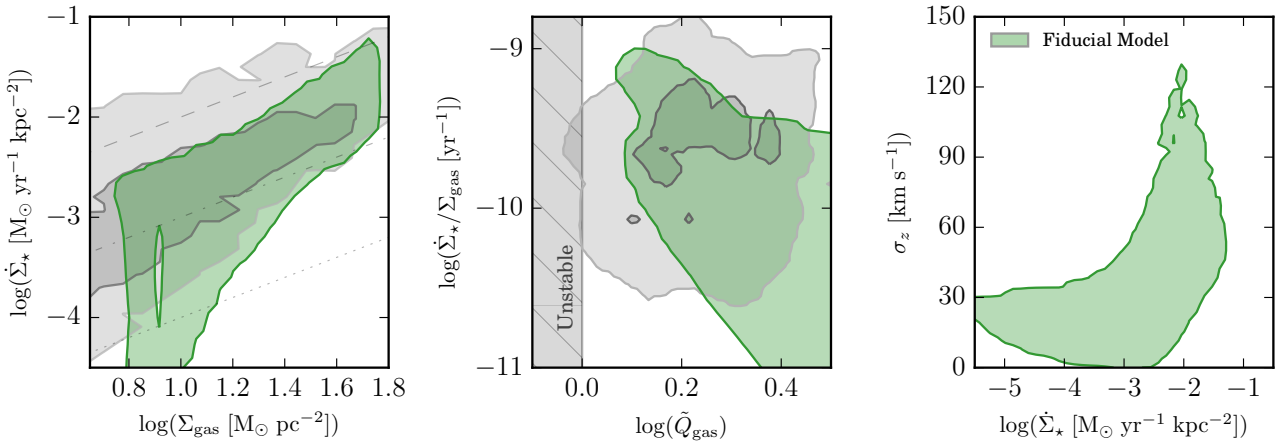

Figure 2. Fiducial model Kennicutt-Schmidt **(top)**, gas depletion time—Toomre-Q **(middle)**, and gas velocity dispersion—SFR **(bottom)** relations for the fiducial parameters listed in Table 2. The light and dark grey shaded regions in the background of the Kennicutt-Schmidt and gas depletion time—Toomre-Q panels denote the 90% and 50%, respectively, contours of the observational data ranges from Bigiel et al. (2008) and Leroy et al. (2008) (KS and $\tau_{\rm dep}$–$\tilde{Q}_{\rm gas}$ panels, respectively). The dashed, dot-dashed, and dotted lines in the KS panel indicate constant depletion times of 10^9, 10^{10}, and 10^{11} yr, respectively. The hatched grey shaded region to the left in the middle panel denotes the Toomre-unstable region. The fiducial model exhibits good agreement with both the Kennicutt-Schmidt and gas depletion time—stability observations (green shaded regions indicate 90% inclusion contours). The Q-threshold is sufficiently soft with its $f_{\rm sf}(\tilde{Q}_{\rm gas})$ 'leakage' to allow star formation to reverse collapse before reaching Q_0/disk instability itself. The large σ_z above $\dot{\Sigma}_\star \approx 10^{-2}$ $\mathrm{M_\odot\ yr^{-1}\ kpc^{-2}}$ reflects the fact that feedback is sufficient to drive outflows at these SFRs (and turbulence in the cold ISM).

model. And so, $\tilde{Q}_{\rm gas}$ and σ_z are in phase throughout their cycles, by definition since $\tilde{Q}_{\rm gas} \propto \sigma_z$ here, ignoring the relatively weak sigma-dependent γ term in front of $\Sigma_\star$ in $\Sigma_{\rm disk}$. Moreover, given the relative stiffness of the star formation threshold in Toomre-Q (for $\Sigma_g = 15$ $\mathrm{M_\odot\ pc^{-2}}$, the 'stiffness' of $f_{\rm sf}(\tilde{Q}_{\rm gas})$ is $\beta \sim 4.6$), star formation commences and is arrested by feedback before $\tilde{Q}_{\rm gas}$ reaches $Q_0 (= 1)$, after which the delayed effects of feedback play out, driving $\tilde{Q}_{\rm gas}$ and the velocity dispersions to their maximal values before the cycle starts anew. The instantaneous star formation rate (not shown) is nearly completely out of phase with the velocity dispersions and Toomre-Q, rising sharply as $\tilde{Q}_{\rm gas}$ falls and falls nearly as quickly as it rises. The "observable" quantity, the 10 Myr averaged star formation rate (c.f. the Hα SFR tracer), shows how the "observed" star formation rates rise by ∼dex as $\tilde{Q}_{\rm gas}$ approaches its minimal value, before falling as the effects of SNe feedback are felt later in the star formation episode.

Variations in the overall strength of feedback, the timing of feedback, and star formation prescription all affect the shape and magnitudes of the star formation cycles in the model, but largely the aforementioned picture holds so long as the timescale of feedback relative to the dynamical time of the system is short but not effectively instantaneous, and that the magnitude of feedback is insufficient to totally disrupt the system. This therefore applies to both galactic centers and in the outskirts of disks, even where the dynamical time is quite long compared to feedback timescales, so long as the ISM is turbulently regulated.

Figure 2 shows the extent of the star formation cycles in the fiducial model across ∼dex in Σ_g in the Kennicutt-Schmidt, depletion time—stability, and star formation rate—gas velocity dispersion relations. At low Σ_g, the model bifurcates into strong "on" and "off" modes[5] as the effects of feedback from peak star formation rates contribute significantly to the overall momentum budget of the disk (c.f. § 4.2), producing a tail to low SFRs in KS, and a spur to long depletion times and 'high' Toomre-Qs. In σ–$\dot{\Sigma}_\star$ space, this is seen as a flattening of the relation, covering broad ranges in $\dot{\Sigma}_\star$ with little change in σ. The large velocity dispersions in gas seen above $\dot{\Sigma}_\star \approx 10^{-2}$ $\mathrm{M_\odot\ yr^{-1}\ kpc^{-2}}$ reflect the fact that feedback is simultaneously able to drive outflows and turbulence in the cold ISM at these SFRs (Hayward & Hopkins 2017). However, in a multiphase ISM, these high dispersions σ_z would not appear in the cold ISM turbulence as this feedback would instead drive outflows (and thus dispersions in the warm neutral and ionized gas components).

Counter-intuitively – but of central importance to observers – when this model is applied to galaxies as a whole (i.e. many $\lesssim$ kpc patches), it produces little correlation between Toomre-Q (or gas σ_z) and resolved star formation rates for $\dot{\Sigma}_\star \lesssim 10^{-2}$ $\mathrm{M_\odot\ yr^{-1}\ kpc^{-2}}$, above which outflows would be possible (and thus σ_z here would no longer strictly encapsulate turbulence in the cold ISM).

3.1 Variations in the Strength and Timing of Feedback

Figure 3 explores the effects on this model due to variations in the strength, delay time, and duration of feedback.

[5] Regions in an "off" mode of the cycle would likely be counted as entirely non-star forming in observations, given their very low SFRs.

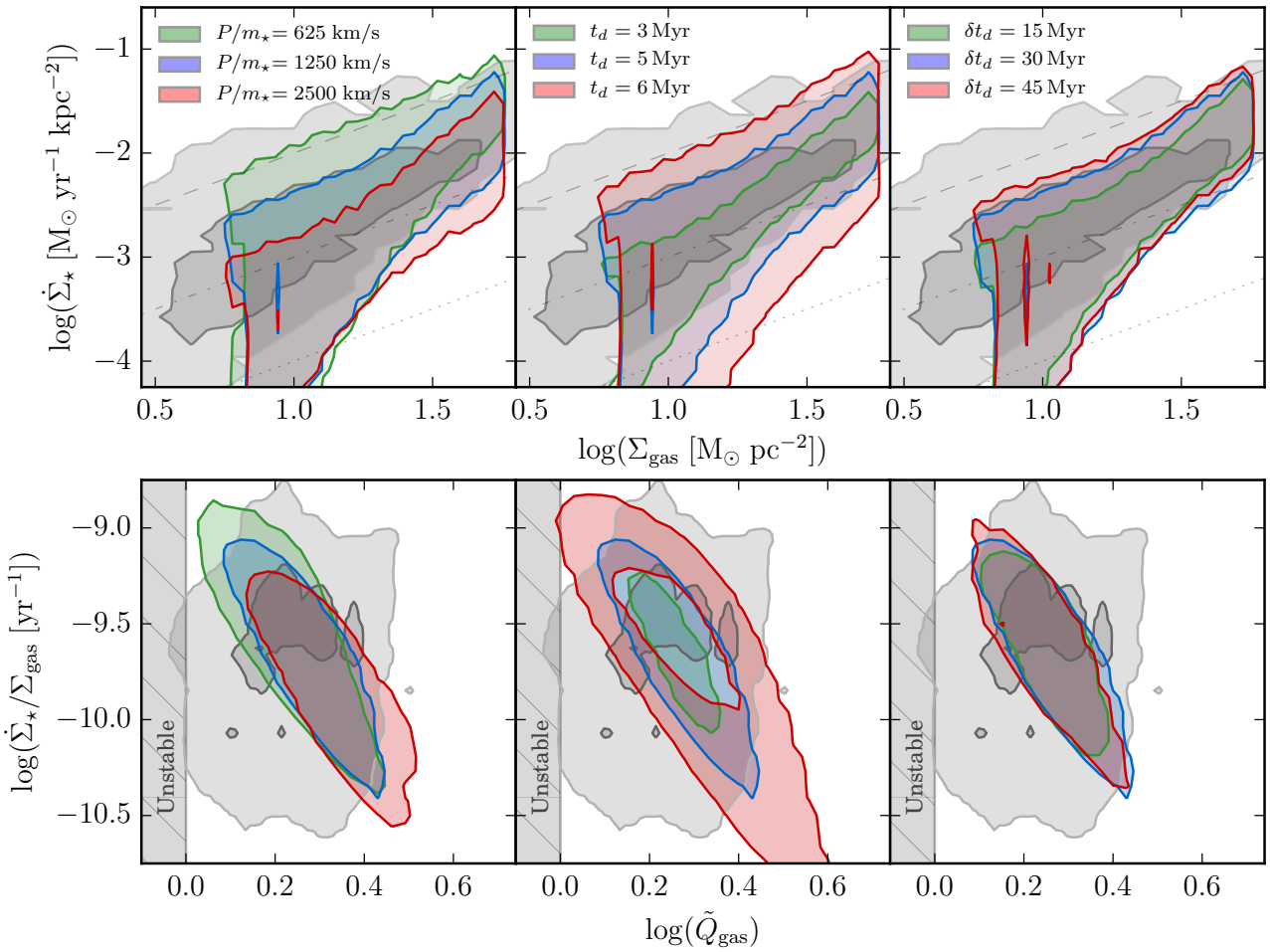

Figure 3. Effects on the Kennicutt-Schidt **(top row)** and depletion time–stability **(bottom row)** relations due to variations **(columns)** in the overall strength ($P/m_\star$), delay time (t_d) and duration (δt_d) of SNe feedback in the fiducial model for $3 < t\Omega < 8$. Background light and dark grey shaded regions and dashed lines represent observational data and lines of constant depletion time, respectively, in the style of Figure 2. **(Top row)** Foreground colored shaded regions denote 90% inclusion intervals for the model; **(bottom row)** shaded regions denote 90% inclusion intervals for > 20 $\mathrm{M}_\odot$ pc^{-2} gas surface densities. **(Left)** Raising (lowering) the overall strength of feedback per mass of stars formed, $P/m_\star$, systematically lowers (raises) the peak/integrated star formation rates in the KS relation and weakly raises (lowers) the gas velocity dispersion distribution. **(Middle)** The delay timescale before the first SNe feedback is injected, t_d, is the strongest factor in determining the departures from SF equilibrium and their magnitudes. Longer delays produce larger departures from equilibrium, that is, larger scatter in SFRs and Toomre-Qs (i.e. velocity dispersions). For the longest delay time, 6 Myr, a clear orbit is seen in the lower panel. **(Right)** Varying the period over which SNe momentum is injected by a single stellar population, δt_d, smoothes out the sharpness of SNe feedback. The effect is small, but longer durations effectively weaken feedback.

3.1.1 Feedback Strength $P/m_\star$

The left column of Figure 3 shows the effects of varying the overall strength of feedback, $P/m_\star$, in our fiducial model: we plot both the Kennicutt-Schmidt relation (relating gas mass and star formation rate surface densities) and the depletion time–Toomre-Q relation (effectively gas consumption efficiency versus stability). As demonstrated extensively in previous works exploring the feedback-regulated regime, variation in the overall strength of feedback primarily effects the equilibrium star formation rates where gas self-regulates: stronger (weaker) feedback yields lower (higher) overall star formation rates (Hopkins et al. 2011, 2012; Shetty & Ostriker 2012b; Agertz et al. 2013; Hopkins et al. 2014; Orr et al. 2018). By construction, this model follows this paradigm. For $\Sigma_g > 20$ $\mathrm{M}_\odot$ pc^{-2}, somewhat larger scatter is driven by stronger feedback, in addition to affecting the overall normalization of the star formation rate distributions. It does affect the minimum velocity dispersions (Toomre-Qs) achieved, as lower feedback strengths take longer to arrest and reverse the run-down of turbulence and disk scale heights (hence elevated star formation overall).

3.1.2 Feedback Delay Time t_d and Duration δt_d

The middle and right columns of Figure 3 show the effects of varying the delay timescale t_d for the first SN feedback (i.e. the lifetime of the most massive star formed in a star formation event, plus the time required to propagate the SNe remnant into the ISM and drive turbulence), and the duration of SN feedback δt_d (i.e. the difference in stellar lifetimes between the least and most massive stars to undergo a Type II SN in a star formation event). The scatter in star formation rates is directly affected by the delay time t_d, with

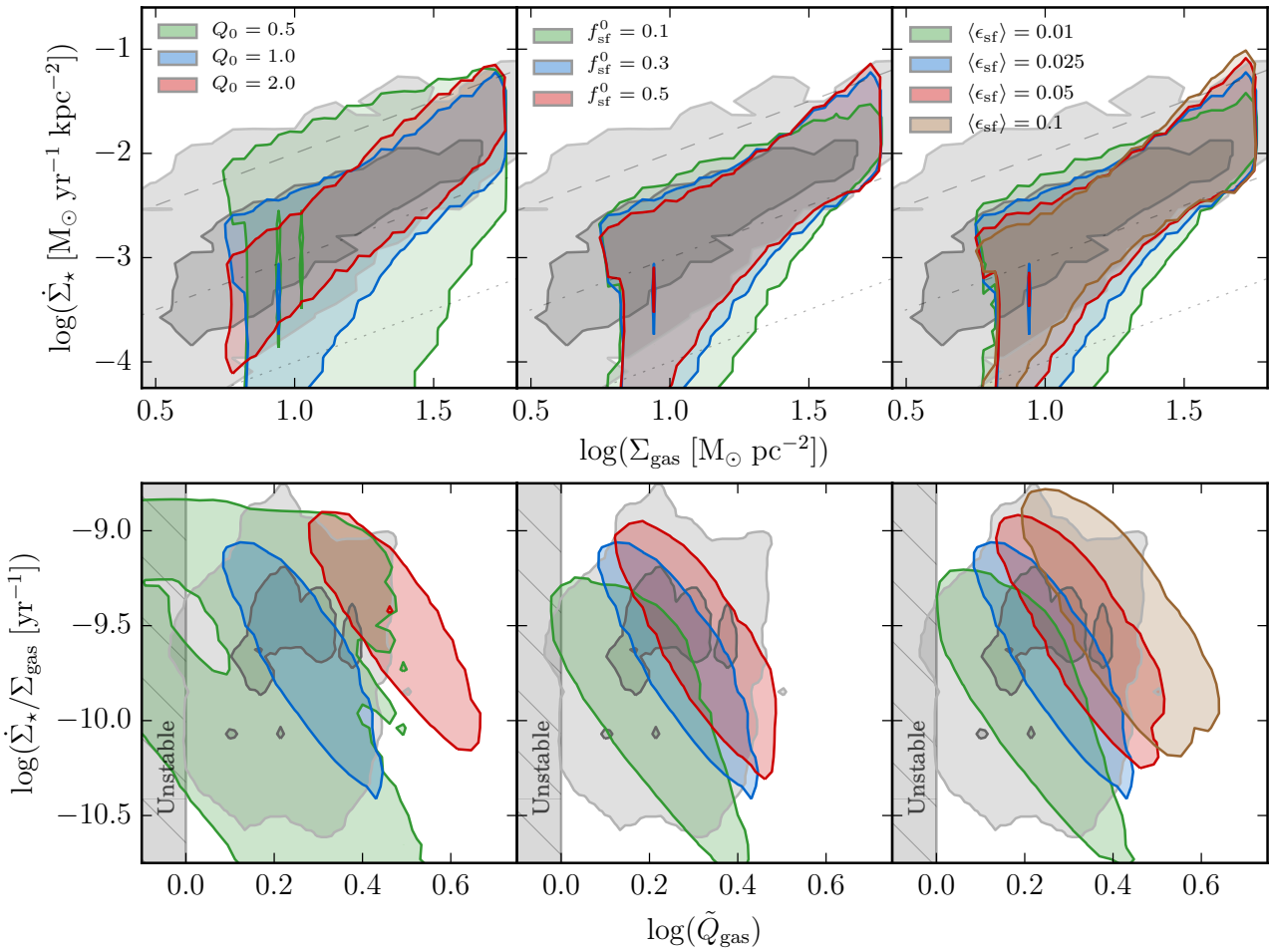

Figure 4. Effects on the Kennicutt-Schmidt **(top row)** and depletion time–stability **(bottom row)** relations due to variations **(columns)** in the Toomre-Q threshold (Q_0), maximal star-forming phase fraction ($f_{\rm sf}^0$), and average local star formation efficiency ($\langle\epsilon_{\rm sf}\rangle$). Plotted quantities and observational data regions are in the style of Figure 3. **(Left)** Shifting $Q_0 = 1 \rightarrow 2$ moves the distributions in depletion time—stability space by ~ 0.3 dex, effectively renormalizing the velocity dispersions that underpin otherwise-constant KS relations. At lower gas surface densities (and everywhere in the $Q_0 = 0.5$ case), the scatter in SFR grows with smaller Q_0; here, feedback injection accounts for a larger fraction of the ISM momentum budget, and star formation episodes are less stable cycles than explosive events (see §4.2). **(Middle)** Varying the maximum fraction of gas in the star-forming phase $f_{\rm sf}^0$ is largely unimportant to the KS relation, as long as it does not "choke" the amount of gas that would otherwise enter the star-forming phase, but shifts distributions in depletion time—stability space: lower maximum star-forming fractions require lower values of $\tilde{Q}_{\rm gas}$ (i.e. higher gas densities) to achieve the same SFR. **(Right)** Higher local star formation efficiencies $\langle\epsilon_{\rm sf}\rangle$ steepen the peak SFRs in the KS relation and shift the distributions in depletion time—stability space (higher efficiencies mean smaller quantities of unstable gas yield the same SFR). For low gas surface densities ($< 10\ {\rm M}_\odot\ {\rm pc}^{-2}$), lower efficiencies result in higher scatter in SFR.

shorter delays producing less scatter in star formation rates. Longer delay times allow for gas to over-produce stars to a greater extent before feedback is felt, hence larger departures from star formation equilibrium. Physically reasonable values of $t_d \sim 3 - 5$ Myr, with a $t^{-0.46}$ weighting, are generally capable of driving $\gtrsim$dex variations in star formation rates.

In a similar vein, shorter feedback durations, δt_d, cause effectively burstier overall feedback and, as such, drive larger scatters in star formation rates. For reasonable feedback durations of $\sim$30 Myr (roughly the difference between the lifetimes of an 8 $M_\odot$ and 40 $M_\odot$ star) the model converges on $\sim$dex scatter in star formation rates. Longer durations smooth out feedback to the extent that it is equivalent in effect to lowering the overall strength of feedback $P/m_\star$.

3.2 Variations in Star Formation Rate Model

To bake a strüdel, one must first cook the filling. Analogously, in order to generate stellar feedback in a model, one must first produce stars. The local star formation rate implemented in this model, Eq. 12, has two principle components that we investigate. Namely, the gas fraction in the star-forming phase $f_{\rm sf}(\tilde{Q}_{\rm gas}; Q_0, f_{\rm sf}^0, \beta)$ (Eq. 11), and the average local star formation efficiency per free-fall time $\langle\epsilon_{\rm sf}\rangle$.

Varying the star formation model (i.e. the local efficiency of star formation and the Toomre-Q threshold for the onset of star formation) has larger systematic effects on the results of our model in depletion time–stability space compared to the effects of reasonable variations in the feedback implemented demonstrated in the previous subsection.

3.2.1 *Toomre-Q Threshold for Star Formation Q_0*

The left column of Figure 4 demonstrates the effects of the particular choice of the Toomre-Q threshold Q_0 on the Kennicutt-Schmidt and depletion time–Toomre-Q relations. For physically reasonable values, the threshold sets the values of the equilibrium velocity dispersions that the models oscillate about.

Larger values of Q_0 produce less scatter in the Kennicutt-Schmidt relation, as Q_0 sets the overall amount of turbulent momentum in the ISM ($\sim \Sigma_g \sigma(\tilde{Q}_{\rm gas} = Q_0)$) where star formation occurs and thus dictates the extent to which star formation events can perturb the ISM at a given Σ_g (see § 4.2 for more rationale). When $Q_0 = 0.5$, the model breaks down even for $\Sigma_g > 20$ M$_\odot$ pc^{-2}, as feedback is able to at least double the momentum in the ISM after every star formation episode. For values of Q_0 where the model holds reasonably well ($Q_0 \gtrsim 1$), doubling $Q_0 = 1 \rightarrow 2$ produces an expected ~ 0.3 dex shift in the Toomre-Q distribution without greatly affecting depletion times (beyond a slight tightening of the SFR distribution): gas is still able to self-regulate (c.f. the predictions of Krumholz & Burkhart 2016).

3.2.2 *Variations in the Maximum Star-forming Fraction $f_{\rm sf}^0$*

In this model, we consider that at the onset of disk scale height gravitational instabilities ($\tilde{Q}_{\rm gas} = Q_0$), there is a maximum mass fraction $f_{\rm sf}^0$ of the ISM participating in star formation. Such a constant has been adopted before in analytic models of feedback regulation in disks (Faucher-Giguere et al. 2013). As seen in the middle column of Figure 4, we see that so long as this factor $f_{\rm sf}^0$ does not 'choke' the fraction of material in the star-forming phase, variations have rather small effects qualitatively. This 'choking' appears to occur at high gas surface densities where choices of small maximal fractions ~ 0.1 clip the maximum SFRs acheived, whereas larger values of $f_{\rm sf}$ do not appear to be the limiting factor on setting maximal SFRs. Larger values of $f_{\rm sf}^0$ move the distributions in depletion time–stability space to shorter depletion times and higher Toomre-Q values; this is the result of renormalizing the "leakage" curve the model follows as $\tilde{Q}_{\rm gas}$ evolves (Eq. 11).

3.2.3 *Variations in Instantaneous Star Formation Efficiency $\langle \epsilon_{\rm sf} \rangle$*

The right column of Figure 4 shows how variations from $\langle \epsilon_{\rm sf} \rangle = 0.01$ to $\langle \epsilon_{\rm sf} \rangle = 0.1$ affect the Kennicutt-Schmidt relation, and gas depletion times and stability (Toomre-Q). Interestingly, variations in the local efficiency over a dex change the maximal star formation rates by $\lesssim 0.5$ dex in opposite directions for high and low gas surface densities. In the feedback regulated regime[6], so long as the local efficiency factor is above that required to produce *enough* stars to inject the appropriate amount of feedback in the ISM to achieve equilibrium, $\langle \epsilon_{\rm sf} \rangle$ should not affect the large-scale, time-averaged star formation rates. However, lower star formation efficiencies do mean that gas must collapse to higher surface densities (i.e. reduced free-fall times) to counteract smaller local efficiencies in order to maintain the momentum balance. This may help raise SFRs at low gas surface densities, but for high gas surface densities, free-fall times are already short compared to the dynamical time. More, as the gas collapses further, but does not produce more momentum in feedback overall (to first order), the distributions in depletion time–stability space for $\Sigma_g > 20$ M$_\odot$ pc^{-2} gas shift, requiring a less stable ISM generally to support the same SFRs with lower star formation efficiencies (moving by ~ -0.2 dex in $\tilde{Q}_{\rm gas}$ and increasing by ~ 0.5 dex in depletion time for a dex change in $\langle \epsilon_{\rm sf} \rangle$).

This suggests that the Kennicutt-Schmidt relation is not a sensitive probe of smaller scale star formation efficiency, but rather that observations in depletion time–stability (Toomre-Q) space have a greater ability to distinguish between low and high local star formation efficiencies in the framework of feedback regulation. Our model favors low cloud-scale average star formation efficiencies $\langle \epsilon_{\rm sf} \rangle \sim 0.01 - 0.1$, as the depletion time–stability constraints otherwise exclude $\langle \epsilon_{\rm sf} \rangle \gtrsim 0.1$.

[6] See Semenov et al. (2018) for a recent discussion of the relative differences between feedback-regulated and dynamics-regulated star formation.

4 DISCUSSION

4.1 The "Instantaneous" Feedback Timescales Limit

Much of this work focuses on the case where the feedback delay timescales t_d and $t_d + \delta t_d$ are within an order of magnitude of the local dynamical time of the galaxy $1/\Omega$ (or for strongly self-gravitating disks, $1/\sqrt{4\pi G \rho_0}$). In the case where t_d and $\delta t_d \ll 1/\Omega$, however, star formation and feedback can be treated as occurring "instantaneously" after a delay time t_d, compressing all SNe and prompt feedback into a spike at t_d. We too can consider the case when the star formation threshold is very sharp, i.e. $\beta \rightarrow \infty$ such that Eq. 11 becomes

$$f_{\rm sf}(\tilde{Q}_{\rm gas}) = \theta(Q_0 - \tilde{Q}_{\rm gas}) f_{\rm sf}^0 \, , \tag{13}$$

where $\theta(Q_0 - \tilde{Q}_{\rm gas})$ is the Heaviside step function at the star formation threshold of $\tilde{Q}_{\rm gas} = Q_0$. In this setting, the turbulent velocity dispersion σ is not allowed to fall much below the threshold value at Q_0, since feedback acts effectively instantaneously once star formation begins to occur.

Thus, the amount of star formation that occurs in a star formation episode is just the amount that can form in one feedback timescale. So, we form an amount of stars per event

$$\Delta\Sigma_\star = \langle \epsilon_{\rm sf} \rangle \, f_{\rm sf}^0 \Sigma_g t_d / t_{\rm eddy} \, . \tag{14}$$

Interestingly, the amount of stars formed has no (direct) relation to the absolute strength of feedback, so long as the amount of momentum eventually injected back into the ISM from this mass of stars is enough to at least momentarily halt additional star formation. The time between star formation events is dependent on the fact that each event will pump up the turbulent velocity dispersion by $\Delta\sigma = (P/m_\star)\Delta\Sigma_\star/\Sigma_g$.

This extra momentum, above that required strictly to maintain stability, takes a time t_{cycle} to decay back down to the star formation threshold $\sigma(\tilde{Q}_{\rm gas} = Q_0)$ of

$$t_{cycle} = \ln(1 + \Delta\sigma/\sigma(\tilde{Q}_{\rm gas} = Q_0))/\Omega \ . \quad (15)$$

It is worth noting, that for the outskirts of galaxies, where the quantity $t_d\Omega$ is likely to be small as we assumed ($1/\Omega$ being the dominant component of the local dynamical time, thanks to exponentially falling disk surface densities), galaxy disks are seen to have relatively constant HI disk velocity dispersions (Tamburro et al. 2009), and so we expect the ratio of $\Delta\sigma/\sigma(\tilde{Q}_{\rm gas} = Q_0)$ to be small. Thus, we can approximate t_{cycle} as $t_{cycle} \approx \Delta\sigma/\sigma(\tilde{Q}_{\rm gas} = Q_0)\Omega$.

And so the average star formation rate over a star formation cycle[7] is $\bar{\dot{\Sigma}}_\star = \Delta\Sigma_\star/t_{cycle}$. Explicitly,

$$\bar{\dot{\Sigma}}_\star \approx \frac{\Sigma_g\Omega\sigma(\tilde{Q}_{\rm gas} = Q_0)}{P/m_\star} \ . \quad (16)$$

The average efficiency of star formation per dynamical time is then

$$\bar{\epsilon}_{\rm sf} = \frac{\bar{\dot{\Sigma}}_\star}{\Sigma_g\Omega} \approx \frac{\sigma(\tilde{Q}_{\rm gas} = Q_0)}{P/m_\star} \ . \quad (17)$$

Neither the average star formation rate nor the average star formation efficiency have an explicit dependence on the "small scale" (GMC-scale) star formation efficiency (here, $\langle\epsilon_{\rm sf}\rangle$) or eddy-crossing/free-fall time $t_{\rm eddy}$, or feedback delay timescale t_d (provided $t_d\Omega \ll 1$), so long as the amount of stars formed in a star formation episode injects enough momentum to regulate the ISM but not enough to fully disrupt it (i.e. pump to very large $\tilde{Q}_{\rm gas}$'s). Unsurprisingly, this is identical to the result of § 2.1, though we are considering a case of extreme dis-equilibrium. This is complementary to the picture of feedback regulation in Semenov et al. (2018), where low star formation efficiencies produce high duty cycles of star formation- after all, less stars formed means $\Delta\sigma/\sigma(\tilde{Q}_{\rm gas} = Q_0)$ will be smaller. Plugging in 'typical' values for $\sigma(\tilde{Q}_{\rm gas} = Q_0) \approx 15 - 30$ km/s and $P/m_\star \approx 1500$ km/s yields a global, averaged star formation efficiency of $\bar{\epsilon}_{\rm sf} \approx 0.01 - 0.02$. These are not altogether unreasonable values for the star formation efficiency in the outskirts of galaxies (Bigiel et al. 2010), and this provides a reasonable mechanism, reliant on averaging non-equilibrium star formation episodes, for regulating *local* star formation (of any efficiency) to global inefficiency on dynamical timescales.

4.2 Low Gas Surface Density Regime/Limit

Seen clearly across the Kennicutt-Schmidt panels of Figures 3 and 4, the delayed feedback model drives large ~ 2 dex scatter in SFRs for gas surface densities $\lesssim 10$ M$_\odot$ pc^{-2}. As the gas surface density falls below 10 M$_\odot$ pc^{-2}, two processes dovetail to make our feedback regulated turbulent disk model break down.

Below ~ 10 M$_\odot$ pc^{-2}, the gas disk transitions from a turbulently-supported molecular disk, to a thermally supported atomic disk, as the sound speed of 10^4 K gas is sufficient with $c_s \sim 11$ km/s to maintain $\tilde{Q}_{\rm gas} \sim 1$. Thus, stirring due to supernovae either aids in keeping gas warm, or is superfluous, as ionizing radiation alone can maintain gas at 10^4 K. (This is not included in the model, as it would require modeling the molecular gas fraction $f_{\rm H_2}$, which is beyond the scope of this work).

On the other hand, for the "lightest" cold, turbulently-supported disks with surface densities ~ 10 M$_\odot$ pc^{-2}, SNe feedback from star formation events can significantly increase the absolute amount of turbulent momentum in the disk. Take a star formation event at a gas surface density of 10 M$_\odot$ pc^{-2} where the disk patch maintains $\dot{\Sigma}_\star \sim 10^{-2}$ M$_\odot$ kpc^{-2} yr^{-1} for 10^7 yr (i.e. the timescale traced by our time-averaged tracer in this paper) producing $\sim 10^5$ M$_\odot$ kpc^{-2} of stars. These young stars then result in a SNe density of $\sim 10^3$ kpc^{-2} in the proceeding ~ 40 Myr (given a rate of a single SNe per 100 M$_\odot$ of stars formed; Ostriker et al. 2010). At a momentum per Type-II SNe of $\sim 10^5$ M$_\odot$ km/s (Martizzi et al. 2015), this is a turbulent momentum injection of $\sim 10^8$ M$_\odot$ km/s kpc^{-2}. For a ~ 10 M$_\odot$ pc^{-2} gas disk, with $\tilde{Q}_{\rm gas} \sim 1$ ($\sigma \sim 10$ km/s), the total turbulent gas momentum is $\sim \Sigma_g\sigma(\tilde{Q}_{\rm gas} \sim 1) \sim 10^8$ M$_\odot$ km/s kpc^{-2}. As the momentum injected approaches the momentum contained in the turbulence field of the whole disk patch, feedback becomes increasingly disruptive to the disk structure. This is more or less the difference between SNe clusters blowing holes in the ISM (dominating), versus churning or stirring it (perturbations).

For these reasons, in the bottom panels of Figures 3 and 4, we include a darker outlined region indicating the depletion time—Toomre-Q space traced by gas only with $\Sigma_g > 20$ M$_\odot$ pc^{-2} where SNe feedback from an individual event does not dominate the momentum budget of the ISM (c.f. here and § 4.1), but is instead responsible for driving stable ∼dex cycles in star formation rates.

5 CONCLUSIONS

In this paper, we developed a simple, non-equilibrium model of star formation in the context of sub-kpc patches of disk galaxies (c.f. local disk scale heights) and explored its ability to explain the scalings and scatter in galaxy star formation relations. Our principal conclusions are as follows:

- The observed Toomre-Q and gas velocity dispersion σ values are not easily connected with observed SFRs (see the bottom panel of Figure 2), as local SFRs may lag either by a considerable fraction of the period of the star formation cycles (i.e. the local free-fall/eddy-crossing time of the disk). Although in this model, the evolution of the resolved instantaneous star formation rate is dictated by local disk conditions, there is very little instantaneous *observable* correlation between the SFR and those disk conditions.
- Longer delay times t_d between star formation and the injection of feedback are able to drive larger departures from star formation equilibrium. This occurs because the ISM is able to "overshoot" and over-produce stars to a greater extent, and the subsequent feedback events drive larger velocity dispersions (Toomre-Qs). Delay times on the order of 3-5 Myr produce ∼dex scatter in SFRs.
- The Kennicutt-Schmidt relation is not sensitive to sub-kpc, GMC or cloud-scale star formation efficiencies. However, the "small-scale" efficiencies can produce effects on the distributions in depletion time–stability (Toomre-Q) space.

[7] This is identical to averaging it over a dynamical time, as then we have a star formation rate of $\Delta\Sigma_\star\Omega/\Omega t_{cycle} = \Delta\Sigma_\star/t_{cycle}$.

The proposed non-equilibrium star formation model can explain the observed $\gtrsim 1$ dex scatter resolved star formation scaling relations. More so than the effects of metallicity or variations in gas fraction, non-equilibrium states of star formation can explain large variations in average star formation rates (e.g. Hα-inferred SFRs). This arises due to the fact that the interplay of bursty feedback, injected over some finite timescale, and the roughly smooth dissipation of turbulence (on ∼kpc scales) struggles to find a stable balance on timescales of tens of Myrs.

Future work using resolved galaxy surveys, like the MaNGA and SAMI surveys, at the sub-kpc scale may help to elucidate the extent to which the scatter in resolved star formation rates correlates with dynamical conditions at the disk scale. The ability to marshal statistically significant samples of star-forming regions with similar physical conditions may make it possible to disentangle potentially confounding local quantities such as metallicity or gas fraction.

ACKNOWLEDGMENTS

MEO is grateful for the encouragement of his late father, SRO, in studying astrophysics. MEO is supported by the National Science Foundation Graduate Research Fellowship under Grant No. 1144469. The Flatiron Institute is supported by the Simons Foundation. Support for PFH was provided by an Alfred P. Sloan Research Fellowship, NASA ATP Grant NNX14AH35G, and NSF Collaborative Research Grant #1411920 and CAREER grant #1455342. This research has made use of NASA's Astrophysics Data System.

REFERENCES

Agertz O., Kravtsov A. V., 2015, Astrophys. J., 804, 18
Agertz O., Kravtsov A. V., Leitner S. N., Gnedin N. Y., 2013, Astrophys. J., 770, 25
Benincasa S. M., Wadsley J., Couchman H. M. P., Keller B. W., 2016, Mon. Not. R. Astron. Soc., 462, 3053
Bigiel F., Leroy A., Walter F., Brinks E., de Blok W. J. G., Madore B., Thornley M. D., 2008, Astron. J., 136, 2846
Bigiel F., Leroy A., Walter F., Blitz L., Brinks E., De Blok W. J. G., Madore B., 2010, Astron. J., 140, 1194
Boehm-Vitense E., 1992, Introduction to stellar astrophysics. Vol. 3 - Stellar structure and evolution
Bolatto A. D., Wolfire M., Leroy A. K., 2013, Annu. Rev. Astron. Astrophys., 51, 207
Calzetti D., Liu G., Koda J., 2012, Astrophys. J., 752, 98
Elmegreen B. G., 2018, Astrophys. J., 854, 16
Elmegreen B. G., Hunter D. A., 2015, Astrophys. J., 805, 145
Faucher-Giguere C.-A., Quataert E., Hopkins P. F., 2013, Mon. Not. R. Astron. Soc., 433, 1970
Federrath C., et al., 2017, Mon. Not. R. Astron. Soc., 468, 3965
Fielding D., Quataert E., Martizzi D., Faucher-Giguère C.-A., 2017, Mon. Not. R. Astron. Soc. Lett., 470, L39
Gilmore G., Reid N., 1983, Mon. Not. R. Astron. Soc., 202, 1025
Grudić M. Y., Hopkins P. F., Faucher-Giguère C.-A., Quataert E., Murray N., Kereš D., 2018, Mon. Not. R. Astron. Soc., 475, 3511
Hayward C. C., Hopkins P. F., 2017, Mon. Not. R. Astron. Soc., 465, 1682
Ho I.-T., et al., 2017, Astrophys. J., 846, 39
Hopkins P. F., 2013, Mon. Not. R. Astron. Soc., 430, 1653
Hopkins P. F., Quataert E., Murray N., 2011, Mon. Not. R. Astron. Soc., 417, 950
Hopkins P. F., Quataert E., Murray N., 2012, Mon. Not. R. Astron. Soc., 421, 3488
Hopkins P. F., Kere D., Onorbe J., Faucher-Giguere C.-A., Quataert E., Murray N., Bullock J. S., 2014, Mon. Not. R. Astron. Soc., 445, 581
Hopkins P. F., et al., 2018, Mon. Not. R. Astron. Soc., 477, 1578
Kennicutt R. C., Evans N. J., 2012, Annu. Rev. Astron. Astrophys., 50, 531
Kennicutt, Jr. R. C., et al., 2007, Astrophys. J., 671, 333
Kim C.-G., Ostriker E. C., 2015a, Astrophys. J., 802, 99
Kim C.-G., Ostriker E. C., 2015b, Astrophys. J., 815, 67
Kruijssen J. M. D., Longmore S. N., 2014, Mon. Not. R. Astron. Soc., 439, 3239
Kruijssen J. M. D., Schruba A., Hygate A. P. S., Hu C.-y., Haydon D. T., Longmore S. N., 2018, Mon. Not. R. Astron. Soc., 50, 1
Krumholz M. R., 2014, Phys. Rep., 539, 49
Krumholz M. R., Burkhart B., 2016, Mon. Not. R. Astron. Soc., 458, 1671
Krumholz M. R., McKee C. F., Tumlinson J., 2009a, Astrophys. J., 693, 216
Krumholz M. R., McKee C. F., Tumlinson J., 2009b, Astrophys. J., 699, 850
Leitherer C., et al., 1999, Astrophys. J. Suppl. Ser., 123, 3
Leroy A. K., Walter F., Brinks E., Bigiel F., de Blok W. J. G., Madore B., Thornley M. D., 2008, Astron. J., 136, 2782
Leroy A. K., et al., 2013, Astron. J., 146, 19
Leroy A. K., et al., 2017, Astrophys. J., 846, 71
Ma X., Hopkins P. F., Wetzel A. R., Kirby E. N., Anglés-Alcázar D., Faucher-Giguère C.-A., Kereš D., Quataert E., 2017, Mon. Not. R. Astron. Soc., 467, 2430
Martizzi D., Faucher-Giguere C.-A., Quataert E., 2015, Mon. Not. R. Astron. Soc., 450, 504
McKee C. F., Parravano A., Hollenbach D. J., 2015, Astrophys. J., 814, 13
Murray N., Quataert E., Thompson T. A., 2010, Astrophys. J., 709, 191
Narayanan D., Krumholz M. R., Ostriker E. C., Hernquist L., 2012, Mon. Not. R. Astron. Soc., 421, 3127
Offner S. S. R., Clark P. C., Hennebelle P., Bastian N., Bate M. R., Hopkins P. F., Moreaux E., Whitworth A. P., 2014, in , Vol. 24, Protostars Planets VI. University of Arizona Press, pp 1–6, doi:10.2458/azu˙uapress˙9780816531240-ch003, http://muse.jhu.edu/books/9780816598762/9780816598762-9.pdf
Oklopčić A., Hopkins P. F., Feldmann R., Kereš D., Faucher-Giguère C.-A., Murray N., 2017, Mon. Not. R. Astron. Soc., 465, 952
Orr M. E., et al., 2018, Mon. Not. R. Astron. Soc., 478, 3653
Ostriker E. C., Shetty R., 2011, Astrophys. J., 731, 41
Ostriker E. C., McKee C. F., Leroy A. K., 2010, Astrophys. J., 721, 975
Padoan P., Pan L., Haugbølle T., Nordlund ., 2016, Astrophys. J., 822, 11
Rafikov R. R., 2001, Mon. Not. R. Astron. Soc., 323, 445
Raiteri C. M., Villata M., Navarro J. F., 1996, Astron. Astrophys., 315, 105
Robertson B., Goldreich P., 2012, Astrophys. J., 750, L31
Saitoh T. R., Daisaka H., Kokubo E., Makino J., Okamoto T., Tomisaka K., Wada K., Yoshida N., 2008, Publ. Astron. Soc. Japan, 60, 667
Schruba A., Leroy A. K., Walter F., Sandstrom K., Rosolowsky E., 2010, Astrophys. J., 722, 1699
Scoville N. Z., Sanders D. B., 1987, in Hollenbach D. J., Thronson Jr. H. A., eds, Astrophysics and Space Science Library Vol. 134, Interstellar Processes. pp 21–50, doi:10.1007/978-94-009-

3861-8'2
Semenov V. A., Kravtsov A. V., Gnedin N. Y., 2017, Astrophys. J., 845, 133
Semenov V. A., Kravtsov A. V., Gnedin N. Y., 2018
Shetty R., Ostriker E. C., 2012a, Astrophys. J., 754, 2
Shetty R., Ostriker E. C., 2012b, Astrophys. J., 754, 2
Smartt S. J., 2009, Annu. Rev. Astron. Astrophys., 47, 63
Tamburro D., Rix H. W., Leroy A. K., Mac Low M. M., Walter F., Kennicutt R. C., Brinks E., De Blok W. J., 2009, Astron. J., 137, 4424
Thompson T. a., Quataert E., Murray N., 2005, Astrophys. J., 630, 167
Toomre a., 1964, Astrophys. J., 139, 1217
Torrey P., Hopkins P. F., Faucher-Giguère C.-A., Vogelsberger M., Quataert E., Kereš D., Murray N., 2017, Mon. Not. R. Astron. Soc., 467, 2301

APPENDIX A: PARAMETERS OF SUPERNOVA FEEDBACK

The lifetimes of massive (8-40 $M_\odot$) stars that are the progenitors of Type II SNe events are fairly well constrained for our purposes. Furthermore, the slope of the massive end of the stellar initial mass function (IMF) is also well known (see Krumholz 2014; Offner et al. 2014, and references therein). Together, these constraints put a strong prior on the parameter space to be explored by this model, in terms of the delay time to the first effects of SNe feedback being felt, how long feedback events last, and the relative distribution of feedback injection in time after a star formation event.

From stellar evolution theory, the main sequence lifetimes of the most massive stars in the local universe range from approximately 4.5 to 38 Myr for 40 to 8 $M_\odot$ stars (Raiteri et al. 1996). We take the lifetime of a 40 $M_\odot$ star as a bound for the minimum delay time to the first SNe feedback effects in our model t_d. Admittedly, longer delay times by perhaps a factor of two are not unreasonable given the (un)likelihood of forming the most massive star first in a local star formation episode, in addition to the various effects rotation and binarity. On the other hand, there is a broader absolute range in the time for the last Type II SNe to go off of 30-49 Myr (approximately factor of two uncertainty), given the uncertainty in the lower mass limit for Type II SNe progenitors of 8 ± 1 $M_\odot$ (Smartt 2009).

To constrain the distribution in time of Type II SNe events from a star formation episode (between the most- and least-massive progenitor's endpoints), i.e. $dN_{\rm SN}/dt$, we combine the IMF slope $dN/dM_\star$ and the mass dependence of main sequence lifetimes (specifically $dt/dM_\star$). Taking the lifetimes of massive stars to be proportional to their mass-to-light ratios $t(M_\star) \propto M_\star/L_\star$ and with $L_\star \propto M_\star^{3.5}$, we have $t(M_\star) \propto M_\star^{-2.5}$ (or $M_\star \propto t^{-2/5}$) and thus $dM_\star/dt \propto t^{-7/5}$ (Boehm-Vitense 1992). From the slope of the high-mass end of the IMF, we take the canonical Salpeter IMF slope of -2.35, i.e. $dN/dM_\star \propto M_\star^{-2.35}$, and in terms of their stellar lifetimes $dN/dM_\star$ is then $\propto t^{4.7/5}$. Combining these arguments, we yield a power-law distribution of,

$$\frac{dN_{\rm SN}}{dt} = \frac{dN}{dM_\star}\frac{dM_\star}{dt} \propto t^{-0.46} , \qquad \text{(A1)}$$

which is fairly weak (though not flat) in time, as the shorter lifetimes of the most massive stars nearly balance out with their relative rarity.

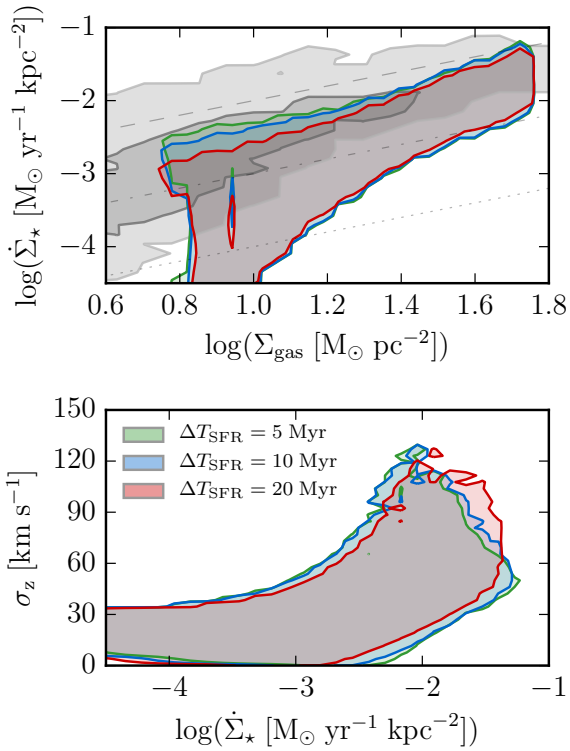

Figure B1. Effects of variation in the star formation averaging period on the model KS and gas velocity dispersions for fiducial model parameters. Observational (KS) data and plotted quantities are in the style of Figure 2. For reasonable choices of averaging period between 5-20 Myr (c.f., the Hα tracer timescale and timescales thereabouts), little to no effect is seen on the average star formation rate distributions. Though longer timescales do smooth out star formation rate peaks at lower gas surface densities somewhat, as the "on" fraction of the star formation duty cycle is the shortest there.

For the purposes of this study, we thus adopt an initial delay time of $t_d = 5$ Myr, a feedback episode period of $\delta t_d = 30$ Myr, and a time-weighting of $dN_{\rm SN}/dt \propto t^{-0.46}$.

APPENDIX B: WHAT ABOUT SFR AVERAGING TIMESCALES?

Observationally, the "instantaneous" star formation rate of a region is ill-defined. YSO counts are perhaps the closest proxy to an true instantaneous star formation rate, but even they are a Myr or more removed from the star formation event itself. As such, any model of non-equilibrium star formation must be convolved with an averaging timescale for the observable tracer. In the case of Hα, we are averaging over a $\sim$ 10 Myr timescale, for tracers like the UV or FIR fluxes, that timescale is significantly longer ($\sim$ 100 Myr). Hence, variability in star formation rates on timescales shorter than the averaging timescale of the particular tracer investigated will be smoothed out. We investigate the effects of particular choices of averaging period $\Delta T_{\rm SFR}$ in Figure B1, wherein we convolve the instantaneous star formation rates produced by our model (Eq. 12) with a 5-20 Myr wide time-averaging window $\Delta T_{\rm SFR}$. Specifically choosing this timescale to be a proxy for the Hα and UV

flux-inferred star formation rates, to show how the variations in SFR over the cycle are smoothed out to varying extents. Increasing the averaging window blunts the star formation rate maxima achieved, as the peak in the star formation cycle is smoothed to some degree. The particular choice of averaging window does not greatly alter the predictions of the model with respect to $\Sigma_{\rm gas}$ or σ_z. The averaging effects on $\dot{\Sigma}_\star$ are relatively small as $\Delta T_{\rm SFR}\Omega \sim 0.35$ in our fiducial model, and so the averaging window constitutes only a fraction of a star formation cycle. Throughout the main body of the text, we adopt a canonical 10 Myr averaging window for our star formation tracer for simplicity.